Available online at www.sciencedirect.com
SCIENCE DIRECT®
ELSEVIER
Nuclear Instruments and Methods in Physics Research B 203 (2003) 116–123
NIM B
Beam Interactions with Materials & Atoms
www.elsevier.com/locate/nimb

Controlling the nanoscale morphology of organic films deposited by polyatomic ions

Luke Hanley [a,*], Yongsoo Choi [a], Erick R. Fuoco [a], F. Ahu Akin [a], Muthu B.J. Wijesundara [a,1], Ming Li [b,2], Aleksey Tikhonov [b,3], Mark Schlossman [a,b]

[a] *Department of Chemistry, University of Illinois at Chicago, M/C 111, 845 W. Taylor Street 4500 SES, Chicago, IL 60607-7061, USA*

[b] *Department of Physics, University of Illinois at Chicago, Chicago, IL 60607, USA*

Abstract

Hyperthermal polyatomic ion beams can be used to fabricate thin film nanostructures with controlled morphology. Several experiments are described in which mass-selected and non-mass-selected polyatomic ion beams are used to create nanometer thick films with controlled surface and buried interface morphologies. Fluorocarbon and thiophenic films are grown on silicon wafers and/or polystyrene from 5 to 200 eV $C_3F_5^+$ or $C_4H_4S^+$ ions, respectively. X-ray photoelectron spectroscopy, atomic force microscopy, X-ray reflectivity, and scanning electron microscopy are utilized to analyze the morphology and chemistry of these films. Polyatomic ions are found to control film morphology on the nanoscale through variation of the incident ion energy, ion structure and/or substrate.

PACS: 31.70.Ks; 68.55.−a; 81.15.Hi; 81.15.Jj
Keywords: Ion-surface; Ion bombardment; Polyatomic ions; Sputtering; Morphology; Nanotechnology

1. Introduction

Polyatomic ions in the hyperthermal energy range (1–500 eV) play a critical role in plasma processing, laser ablation and several other energetic deposition processes [1–3]. Covalently bound polyatomic ions composed of 4–30 atoms are especially important in energetic deposition when organic vapors or polymeric source targets are utilized. Polyatomic ion beams are advantageous for practical surface modification due to their unique collision dynamics and ability to transfer intact chemical functionality to the surface [4,5]. For example, polyatomic ions can often be soft-landed as intact species at $\leqslant 10$ eV collision energies [2,6] or used to create a variety of surface chemical gradients [7]. Polymeric films have been grown from organic ion sources for applications in optoelectronics [8].

* Corresponding author. Tel.: +1-3129960945; fax: +1-3129960431.
E-mail address: lhanley@uic.edu (L. Hanley).
[1] Present address: Department of Chemical Engineering, University of California, Berkeley, CA 94720, USA.
[2] Present address: Institute of Physics, Chinese Academy of Sciences, Beijing 100080, PR China.
[3] Present address: NSLS Beamline X19C, Brookhaven National Laboratory, Upton, NY 11973, USA.

0168-583X/03/$ - see front matter
doi:10.1016/S0168-583X(02)02183-3

Hyperthermal polyatomic ion beams also confine their modification to the top few nanometers of a surface [1,2]. This capability renders polyatomic ions particularly useful for the fabrication of thin film nanostructures with controlled morphology. Several experiments are described below in which mass-selected and non-mass-selected polyatomic ion beams are used to create nanometer thick films with controlled surface and buried interface morphologies. Fluorocarbon and thiophenic films are grown on silicon wafers and/or polystyrene from 5 to 200 eV $C_3F_5^+$ or $C_4H_4S^+$ ions, respectively. X-ray photoelectron spectroscopy (XPS), atomic force microscopy (AFM), X-ray reflectivity, and scanning electron microscopy are utilized to analyze the chemistry and morphology of these films.

2. Experimental methods

Mass-selected ion deposition begins with polyatomic ion formation in an 80 eV electron impact source, in an instrument that has been described previously [4,9]. The polyatomic ions are then accelerated to ~1000 eV, mass-selected by a Wien filter, bent 3°, decelerated and transported to the target at normal incidence and at the appropriate kinetic energy. Typical ion currents for this instrument are 10–100 nA/cm^2 for the various mass-selected ions utilized here, requiring sample preparation times of several hours for a single thin film of a few mm^2 area. The preparation chamber is connected to the monochromatic XPS chamber via a load-lock sample transfer stage. The XPS is equipped with a 600 W AlK_α X-ray gun mounted on a 0.7 m radius Rowland circle monochromator and 150 mm cylindrical hemispherical analyzer equipped with a five channel detector (VSW Ltd., Macclesfield, UK).

Fig. 1 depicts the instrument used for non-mass-selected polyatomic ion deposition. This instrument is equipped with a broad beam Kaufman ion source (Veeco-CS, 3 cm Ion Source) whose gas input is metered by a mass flow controller. The parent ion $C_4H_4S^+$ constitutes over 60% of the ion current from the Kaufman ion source when utilizing thiophene vapor. The high parent ion current is achieved by operating the Kaufman ion source at a relatively low discharge voltage (near the ionization threshold). The thiophene ion current ranges from 0.1 to 5 mA/cm^2 in the Kaufman ion source. This chamber is also equipped with a load-lock sample transfer stage, quartz crystal microbalance, differentially pumped quadrupole mass analyzer (for ion and neutrals analysis), cylindrical mirror analyzer and electron gun for Auger electron spectroscopy and Fourier transform infrared spectrometer for reflection absorption infrared spectroscopy.

Quantitative analysis of surfaces by electron spectroscopy software (QUASES, Tougaard APS, Odense, Denmark) is used to estimate the fluorine and silicon depth profiles for ion-deposited fluorocarbon films on H–Si(1 0 0) [10,11], as described previously [12]. QUASE analyzes the energy loss structure of XP spectra to determine the depth of origin of the detected electrons by fitting to a given surface morphology.

X-ray reflectivity was conducted at beamline X19C at the National Synchrotron Light Source (Brookhaven National Laboratory, USA) with measurement techniques described in detail elsewhere [13,14].

The surface morphology of ion-deposited films is observed using an atomic force microscope (AFM, Nanoscope IIIA, Digital Instruments, Santa Barbara, CA, USA) operating in tapping mode to avoid surface damage. Multiple areas of several microns side dimension are scanned for each sample and the RMS roughness averages calculated for each ion energy. Low voltage scanning electron microscopy is performed at 5.00 keV electron beam energy (Hitachi S3000N VPSEM) on samples that have been cross-sectioned prior to analysis in a microtome. Substrate preparation conditions prior to ion-deposition have been described previously [12,15,16].

3. Results and discussion

3.1. Morphology of fluorocarbon thin films on polystyrene

Fluorocarbon films are grown on a spin-coated polystyrene surface by deposition of 25 or 100 eV

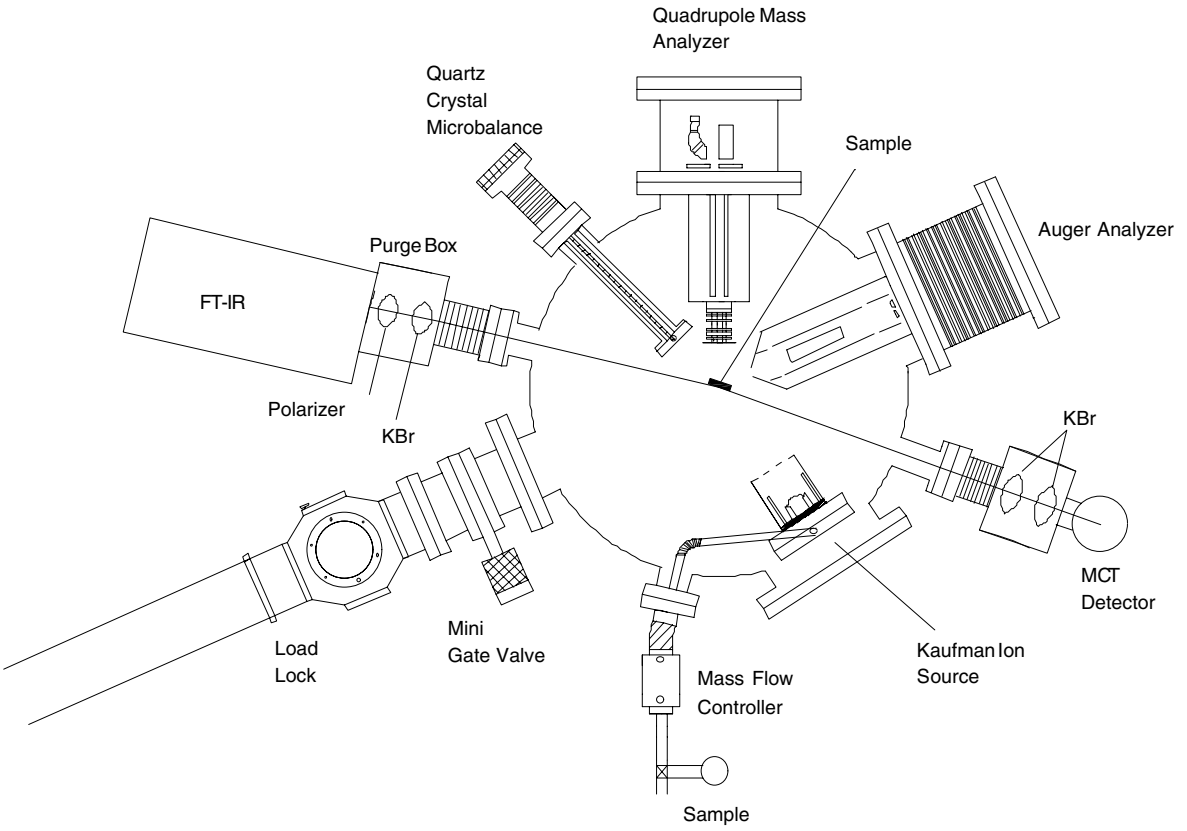

Fig. 1. Schematic diagram of Kaufman ion source instrument for non-mass-selected deposition.

$C_3F_5^+$ ions. Analysis of the film chemistry by XPS finds a strong dependence upon both ion energy and structure, as discussed previously [4,17]. AFM and X-ray reflectivity of these fluorocarbon films and unmodified spin-coated polystyrene demonstrate the ability of mass-selected polyatomic ions to control surface and buried interface morphology.

Fig. 2 includes previously published AFM data ("$C_3F_5^+$/PS") indicating relatively rough surfaces for 100 eV fluorocarbon films, but smoother films deposited at 25 eV [15]. Hillocks in the 100 eV $C_3F_5^+$ fluorocarbon films of ~20 nm diameter and ~1 nm height were observed by AFM. No such hillocks were observed for films deposited by 25 eV $C_3F_5^+$, which displayed feature heights of only ~0.2 nm. The roughness of the unmodified PS surface was ~0.1 nm.

Fig. 3 displays the X-ray reflectivity for the fluorocarbon layer from 25 eV $C_3F_5^+$ deposition on a polystyrene layer spin-coated onto a silicon wafer. Fig. 4 displays the electron density profiles used to fit the X-ray reflectivity data for the three surfaces – native polystyrene, 25 eV fluorocarbon and 100 eV fluorocarbon. Table 1 reports the results of fitting this X-ray reflectivity data.

Oscillations in the X-ray reflectivity for the native polystyrene layer, similar to those shown in Fig. 3, are due to coherent interference between X-rays reflected from the polystyrene–vapor interface and the silicon–polystyrene interface. A single layer model (see Fig. 4) is used to fit this interface and yields a layer thickness of 27.5 nm with an electron density $\rho_{PS} = 0.455\ \rho_{Si}$, where the electron density of the silicon is $\rho_{Si} = 0.696\ e^-/Å^3$. The value for ρ_{PS} compares favorably with the

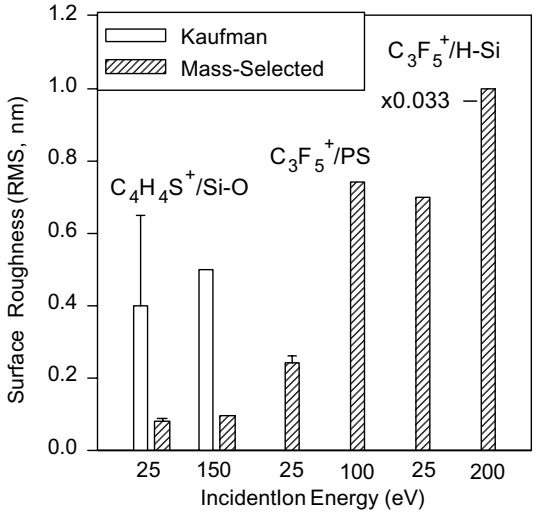

Fig. 2. Surface roughness (RMS) obtained by AFM of various films deposited from hyperthermal, mass-selected or non-mass-selected ("Kaufman") beams of $C_4H_4S^+$ or $C_3F_5^+$ ions. "Si–O" is the native oxide of Si(1 0 0), "PS" is spin coated polystyrene and "H–Si" is hydrogen terminated Si(1 0 0). The roughness of the 200 eV $C_3F_5^+$/Si–O data is scaled by 0.033 to facilitate display.

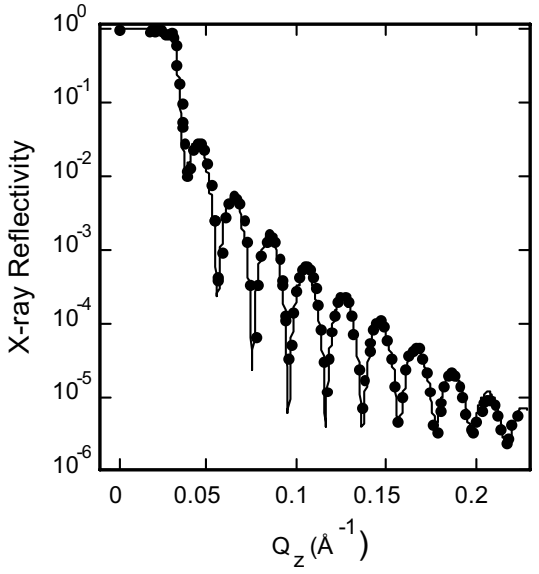

Fig. 3. X-ray reflectivity data (points) and fit (line) as a funtion of wave vector transfer normal to the silicon surface for a spin-coated polystyrene layer on silicon exposed to 25 eV $C_3F_5^+$ ions at an ion fluence equivalent to 1×10^{16} F atoms/cm^2.

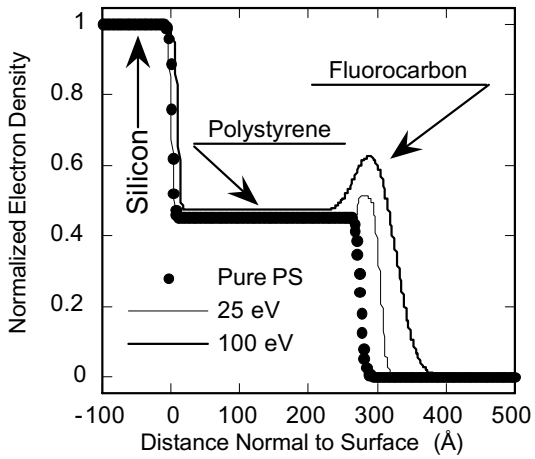

Fig. 4. Electron density profiles used to fit the X-ray reflectivity data for native polystyrene and fluorocarbon films on polystyrene from 25 and 100 eV $C_3F_5^+$ deposition.

value deduced from the literature value for the mass density of 1.0 g/cm^3, which corresponds to $\rho_{\text{literature polystyrene}} = 0.46$ [18]. The width (or roughness) of the vapor interface is 0.55 nm and the width of the polystyrene–Si interface is 0.27 nm.

The fit for the 25 eV fluorocarbon X-ray reflectivity (Fig. 3) is consistent with the AFM results and also provides an indication of the buried interface width (see PS/F interface width in Table 1). The fit shown in Fig. 3 is a two layer model (Fig. 4), since reflectivity of the fluorocarbon layer cannot be adequately fit by a one layer model of polystyrene. The polystyrene layer is similar to the layer on the pure polystyrene sample indicating that it is probably unaltered by exposure to the $C_3F_5^+$ ions. On top of the polystyrene layer is a 3.3 nm thick layer of higher electron density than polystyrene. This is attributed to fluorocarbon, though its electron density, $\rho_F = 0.515\ \rho_{Si}$ is much less than the value measured for close-packed fluoro-alkanes ($0.9\ \rho_{Si}$) [19]. This relatively low electron density indicates either loose packing in the fluorocarbon layer, incomplete fluorocarbon coverage on the polystyrene, or a combination of both effects.

The 100 eV X-ray reflectivity data (not shown) indicates a much thicker 6.0 nm fluorocarbon film with 30% higher electron density than observed for the 25 eV samples. The vapor interface and the

Table 1
Parameters for fitting X-ray reflectivity data for polystyrene spin-coated on silicon and fluorocarbon films on same from 25 and 100 eV $C_3F_5^+$

	Polystyrene	25 eV	100 eV
Layer thickness, L_j (nm)			
SiO_2, L_1			1.0 ± 0.1
Polystyrene, L_2	27.52 ± 0.05	27.2 ± 0.2	25.8 ± 0.3
Fluorocarbon, L_3		3.3 ± 0.3	6.0 ± 0.5
Electron density, ρ_j/ρ_{Si}			
SiO_2, ρ_1/ρ_{Si}			0.96[a]
Polystyrene, ρ_2/ρ_{Si}	0.455 ± 0.015	0.45[a]	0.47 ± 0.1
Fluorocarbon, ρ_3/ρ_{Si}		0.515 ± 0.025	0.68 ± 0.05
Interface width (or roughness), σ_{ij} (nm)			
Si/SiO_2 or Si/polystyrene, σ_{01}	0.27[a]	0.34 ± 0.03	0.1[a]
SiO_2/polystyrene, σ_{12}			0.25 ± 0.01
Polystyrene/F or polystyrene/vapor, σ_{23}	0.55 ± 0.05	0.3 ± 0.3	1.8 ± 0.6
F/vapor, σ_{34}		0.68 ± 0.05	2.25 ± 0.2

Electron densities, ρ, are normalized by ρ_{Si} where $\rho_{Si} = 0.696\ e^-/Å^3$. Other fitting parameters include the critical Q for total reflection from silicon, $Q_C = 0.0318\ Å^{-1}$; X-ray absorption lengths of 0.104 cm for the polystyrene and 0.0066 cm for the silicon. Blank values indicate layers not used (fitting layer numbering adjusts accordingly).

[a] Parameters kept fixed during fitting.

buried interface between the fluorocarbon layer and the polystyrene for the 100 eV films is much rougher at ~2 nm versus 0.3–0.7 nm for the 25 eV films. Fig. 4 displays the electron density of this rougher and thicker fluorocarbon layer from 100 eV $C_3F_5^+$.

These results support the model of a thinner, smoother, lower electron density and possibly discontinuous fluorocarbon film formed from 25 eV $C_3F_5^+$. This is consistent with the chemical composition of these 25 eV films: 20% overall fluorine comprised of 87% CH_n, 8% CCF_n and 4% CF_2 [15]. By contrast, the 100 eV films are rougher, thicker and higher electron density films. The higher electron density of these 100 eV films can be attributed to their chemical content: 40% overall fluorine comprised of 40% CH_n, 38% CCF_n, 15% $CFCF_n$, 7% CF_2 and <1% CF_3. Higher ion energy leads to more penetration and fragmentation of both the incident $C_3F_5^+$ ions and the polystyrene substrate, collectively contributing to the nanostructuring. Differences in the oxidation of these films – ~4% oxygen for the 100 eV films versus ~2% for the 25 eV films – may also play a minor role in the film morphology. The fluorocarbon components of these films are also likely due in part to oxidized species, as previously discussed for fluorocarbon films on polymethylmethacrylate substrates [7].

3.2. Morphology of fluorocarbon thin films on silicon

Morphological control is also demonstrated by fluorocarbon ion deposition onto clean hydrogen terminated Si(1 0 0) surfaces, H–Si(1 0 0). The width of the buried interface between the deposited fluorocarbon film and the Si substrate is also shown here to be controlled by the deposition process. Mass-selected 5–200 eV $C_3F_5^+$ and $C_2F_4^+$ ions are used to form nanometer thick fluorocarbon and $Si_xC_yF_z$ films on H–Si(1 0 0) [12].

XPS shows that the average elemental and chemical content of the deposited film is nearly independent of ion identity and kinetic energy, in stark contrast to the case for polymers (see above). The fluorocarbon film composition for 25–200 eV $C_3F_5^+$ ion deposition is 60% overall fluorine (at saturation ion fluence), comprised of 45% CCF_n, 35% $CFCF_n$, 15% CF_2 and 2–3% CF_3 [12]. Similar film compositions are observed for 25–200 eV $C_2F_4^+$ ion deposition, although the compositions of the 5 eV films deposited from both ions vary slightly. Overall, the chemical nature of the

fluorocarbon films on Si is controlled largely by surface chemical and diffusion processes rather than the ion structure or incident energy.

However, ion energy and structure strongly affect the fluorocarbon film morphology. Fig. 5 displays the fluorine depth profile of nanoscale fluorocarbon films on H–Si(1 0 0) deposited from mass-selected 5–200 eV $C_3F_5^+$ and $C_2F_4^+$ at ion fluences equivalent to 1.5×10^{16} F atoms/cm^2 [12]. XPS depth profiles of the films depend strongly upon ion energy and structure, with the fluorine depth profile extending deeper into the surface at higher ion energies for both $C_3F_5^+$ and $C_2F_4^+$. Furthermore, $C_3F_5^+$ films display a deeper and broader fluorine depth profile when compared with films from isoenergetic $C_2F_4^+$. Finally, overlap of the fluorine and silicon (data not shown) depth profiles indicate formation of a $Si_xC_yF_z$ buried interface of thickness ranging from <1 nm at 5 eV ion energy to >5 nm at 200 eV.

AFM is also employed to investigate the changes in surface morphology associated with $C_3F_5^+$ ion deposition, with roughnesses summarized in Fig. 2 ("$C_3F_5^+$/H–Si"). The roughness of the surface increases to 0.7 nm with 25 eV ion bombardment compared with the <0.2 nm roughness of native H–Si (1 0 0). The RMS roughness of the H–Si(100) surface increases dramatically to ~30 nm after 200 eV ion bombardment (scaled by $\times 0.033$ in Fig. 2). Fig. 6 displays the AFM of

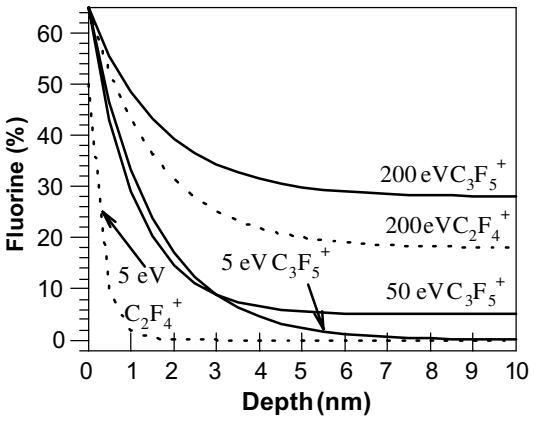

Fig. 5. Fluorine depth profiles for fluorocarbon films on H–Si(1 0 0) deposited from mass-selected 5–200 eV $C_3F_5^+$ and $C_2F_4^+$ at an ion fluence equivalent to 1.5×10^{16} F atoms/cm^2.

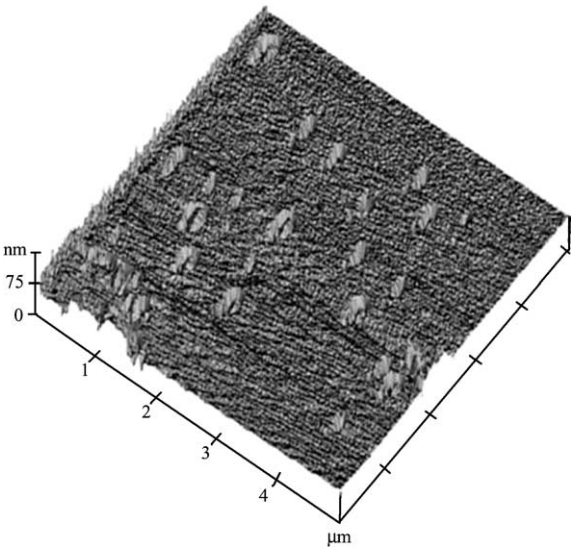

Fig. 6. AFM of 200 eV $C_3F_5^+$ ion deposition on H–Si(1 0 0) at an ion fluence equivalent to 4.5×10^{16} F atoms/cm^2, following air exposure.

200 eV $C_3F_5^+$ ion deposition on H–Si(1 0 0), which leads to the formation of oblong surface pits of average depth of 30 ± 5 nm, width of 120 ± 20 nm and length of 300 ± 200 nm. Some smaller features are also observed with depths $\leqslant 7$ nm. 25 eV $C_3F_5^+$ ion deposition does not form pits on the Si surface, but rather a smooth surface with small hillocks of 3 ± 1 nm height and 230 ± 50 nm diameter.

The morphology of these fluorocarbon films can be explained by comparison with molecular dynamic simulations and studies of fluorocarbon plasma etching of Si [20–22]. A relatively smooth and thick fluorocarbon layer forms at the lowest ion energy of 25 eV, which is mostly insufficient to induce fluorocarbon film mixing with the bulk Si. Penetration of the ions into the substrate at $\geqslant 50$ eV collision energies leads to mixing to form a $Si_xC_yF_z$ interfacial layer. At the highest ion energy of 200 eV, ion penetration into and mixing of the surface layers cause formation of volatile SiF_x, fluorocarbons and fluorine. These volatile species are thought to lead to Si etching, assisted by sputtering processes. This model is generally consistent with molecular dynamics simulations of CF_3^+ ion bombardment of Si, which similarly showed an increase in the $Si_xC_yF_z$ layer depth and

width with increasing ion energy [22]. The different depth profiles for $C_3F_5^+$ and $C_2F_4^+$ can also be explained by consideration of molecular dynamics simulations on CF^+ and CF_2^+ bombardment of Si [23]. By analogy, these simulations suggest that the incident $C_3F_5^+$ ions fragment to form more of the mobile and reactive fluorine atoms upon impact than do $C_2F_4^+$ ions. The >100 nm oblong pits observed at 200 eV ion energies is consistent with etching, but their dimensions are much large than the ~1 nm pits expected to form directly by individual ion impacts. Ion-assisted diffusion and mixing must be occurring here to allow the nucleation and growth of these large etch pits [24].

3.3. Morphology of thiophenic films deposited by mass- and non-mass-selected ions

Thiophenic thin films of controlled surface morphology can also be grown by both mass-selected and non-mass-selected ion beams. Both low current beams of mass-selected ions and high current beams of non-mass-selected ions are utilized for the experiments described below, the latter from a Kaufman ion source (see Fig. 1). The 25 and 150 eV mass-selected ions are deposited at fluences of 1.8 and 0.8×10^{16} ions/cm^2, respectively. The Kaufman ion fluences are $>10^{16}$ ions/cm^2, but exact fluences are not available since the ion currents are not compensated for electron fluxes. XPS is used to elementally analyze these thiophenic films, with the results shown in Fig. 7. Both films are composed of carbon and sulfur in ratios close to molecular thiophene. The films contain no oxygen immediately after formation (''No aging''), but accumulate a few percent oxygen after several weeks of aging in air (''Aged'') (see below). However, the oxygen content is not directly comparable between the two types of films since the Kaufman films aged for 4 weeks and the mass-selected films aged for 8 weeks.

The thicknesses and surfaces morphologies of these thiophenic films are also determined. Both deposition methods produce films thicker than the ~10 nm sampling depth of XPS, indicated by the disappearance of the Si substrate signal (data not shown). Scanning electron microscopy of a cross-section of 5 eV films produced by the Kaufman ion source show film thicknesses of 300–500 nm, indicating film growth rates on the order of 50 nm/min. Films grown at 25 and 150 eV ion energy by either source are found by AFM to be smooth and featureless on the >1 nm scale, as noted in Fig. 2. The Kaufman source films display RMS roughnesses of ~0.5 nm and the mass-selected films are even smoother, with roughnesses of ~0.1 nm. These smooth films contrast with highly structured films evaporated from oligothiophenes [25,26].

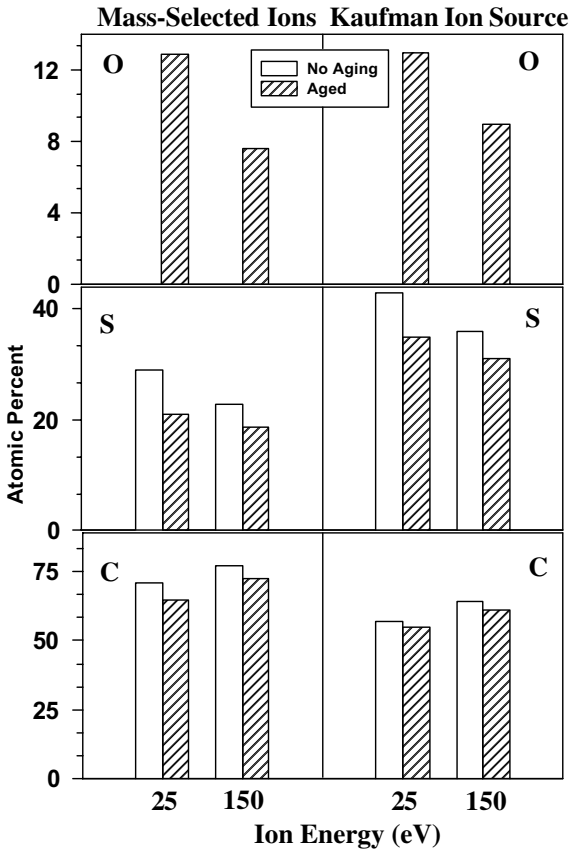

Fig. 7. Elemental analysis by XPS of thiophenic films deposited on the native oxide of Si(1 0 0) from 25 and 150 eV $C_4H_4S^+$ ions from either the mass-selected or Kaufman ion sources. See text for ion fluences.

4. Conclusions

These results demonstrate that hyperthermal polyatomic ion deposition allows control of

nanoscale morphology at the surface and/or buried interface for three different systems. Both mass-selected and non-mass selected ions control film morphology through variation of the ion energy, ion structure and/or substrate. These ion parameters control morphology through their mediation of the competing processes of ion deposition, ion fragmentation, ion penetration into and damage of the substrate, reactions between deposited ions and/or the substrate, sputtering, etching and diffusion. Mass-selected beams allow well-defined experiments that are directly comparable to molecular dynamics simulations, but are practical only for film growth over small areas [4,17,27]. The Kaufman ion source produces thicker films over much larger areas and can be scaled up to a commercial process. However, the Kaufman ion source produces several different ions as well as difficult to quantify radicals, electrons and photons. The latter species also contribute to film growth in manner previously characterized for only a few cases [28,29]. Future experiments will evaluate the role of ion fluence, which is known to be significant in film growth by atomic ions [1,24].

Acknowledgements

This work is supported by the US National Science Foundation through grant CHE-9986226 (L.H.) and DMR-0092469 (M.S.). The X-ray reflectivity experiments were performed at the National Synchrotron Light Source on beamline X19C, Brookhaven National Laboratory, which is supported by the US Department of Energy.

References

[1] L. Hanley, S.B. Sinnott, Surf. Sci. 500 (2002) 500.
[2] D.C. Jacobs, Ann. Rev. Phys. Chem. 53 (2002) 379.
[3] K.L. Williams, I.T. Martin, E.R. Fisher, J. Am. Soc. Mass Spectrom. 13 (2002) 518.
[4] M.B.J. Wijesundara, Y. Ji, B. Ni, S.B. Sinnott, L. Hanley, J. Appl. Phys. 88 (2000) 5004.
[5] C. Evans, N. Wade, F. Pepi, G. Strossman, T. Schuerlein, R.G. Cooks, Anal. Chem. 74 (2002) 317.
[6] N. Wade, C. Evans, S.-C. Jo, R.G. Cooks, J. Mass Spectrom. 37 (2002) 591.
[7] M.B.J. Wijesundara, E. Fuoco, L. Hanley, Langmuir 17 (2001) 5721.
[8] H. Usui, Thin Solid Films 365 (2000) 22.
[9] L. Hanley, H. Lim, D.G. Schultz, S. Garbis, C. Yu, E.T. Ada, M.B.J. Wijesundara, Nucl. Instr. and Meth. B 157 (1999) 174.
[10] S. Tougaard, J. Vac. Sci. Technol. A 14 (1996) 1415.
[11] S. Tougaard, Surf. Interf. Anal. 26 (1998) 249.
[12] E.R. Fuoco, L. Hanley, J. Appl. Phys. 92 (2002) 37.
[13] M.L. Schlossman, D. Synal, Y. Guan, M. Meron, G. Shea-McCarthy, Z. Huang, A. Acero, S.M. Williams, S.A. Rice, P.J. Viccaro, Rev. Sci. Instr. 68 (1997) 4372.
[14] M.L. Schlossman, P.S. Pershan, in: D. Langevin (Ed.), Light Scattering By Liquid Surfaces and Complementary Techniques, Marcel Dekker, New York, 1992, p. 365.
[15] M.B.J. Wijesundara, G. Zajac, E. Fuoco, L. Hanley, J. Adhes. Sci. Technol. 15 (2001) 599.
[16] L. Hanley, E. Fuoco, M.B.J. Wijesundara, A.J. Beck, P.N. Brookes, R.D. Short, J. Vac. Sci. Technol. A 19 (2001) 1531.
[17] M.B.J. Wijesundara, L. Hanley, B. Ni, S.B. Sinnott, Proc. Nat. Acad. Sci. USA 97 (2000) 23.
[18] T.P. Russell, Mater. Sci. Rep. 5 (1990) 171.
[19] H. Schwickert, G. Strobl, M. Kimmig, J. Chem. Phys. 95 (1991) 2800.
[20] J.W. Coburn, J. Vac. Sci. Technol. A 12 (1994) 1417.
[21] G.S. Oehrlein, Surf. Sci. 386 (1997) 222.
[22] C.F. Abrams, D.B. Graves, J. Vac. Sci. Technol. A 18 (2000) 411.
[23] C.F. Abrams, D.B. Graves, J. Vac. Sci. Technol. A 19 (2001) 175.
[24] K.J. Boyd, D. Marton, J.W. Rabalais, S. Uhlmann, T. Frauenheim, J. Vac. Sci. Technol. A 16 (1998) 444.
[25] D. Fichou, C. Ziegler, in: D. Fichou (Ed.), Handbook of Oligo- and Polythiophenes, Wiley–VCH, Weinheim, 1999, p. 185.
[26] C. Taliani, F. Biscarini, M. Muccini, in: G. Hadziioannou, P.F. van Hutten (Eds.), Semiconducting Polymers, Wiley–VCH, Weinheim, 2000, p. 149.
[27] B. Ni, R. Andrews, D. Jacques, D. Qian, M. Wijesundara, Y. Choi, L. Hanley, S.B. Sinnott, J. Phys. Chem. B 105 (2001) 12719.
[28] W. Jacob, Thin Solid Films 326 (1998) 1.
[29] A. von Keudell, Thin Solid Films 402 (2002) 1.